sustainability

MDPI

Review

Constitutive Behaviour of Recycled Rubber-Involved Mixtures for Transportation Infrastructure

Yujie Qi *, Kavishka Wijesooriya, Buddhima Indraratna and A. S. M. Riyad

Transport Research Centre, School of Civil and Environmental Engineering, University of Technology Sydney, Sydney, NSW 2007, Australia; kavishka.h.wijesooriya@student.uts.edu.au (K.W.); buddhima.indraratna@uts.edu.au (B.I.); a.s.riyad@student.uts.edu.au (A.S.M.R.)

* Correspondence: yujie.qi@uts.edu.au

Abstract: The scarcity of natural aggregates and the growing accumulation of waste materials have driven the demand for sustainable and circular economy solutions in transportation infrastructure, and this has led to the utilization of waste materials in transport infrastructure, such as recycled rubber. Although numerous laboratory experiments have been conducted on granular mixtures mixed with rubber, predicting the complex stress–strain behaviour of these mixtures mathematically and capturing the influence of rubber on the geotechnical properties of waste mixtures are imperative. This paper presents a comprehensive review of the constitutive models developed to predict the stress–strain behaviour, dilatancy, and shear strength of rubber-mixed waste materials, including sand–rubber, coal wash–steel furnace slag–rubber crumbs, and coal wash–rubber crumbs in various transport infrastructure applications under static loading. This paper also highlights the innovations and limitations of these existing constitutive models on rubber-mixed materials. It was found that existing constitutive models based on hyperbolic, hypoplastic, critical state, and bounding surface plasticity approaches can capture the behaviour of these materials under static loading conditions. However, further developments are required to incorporate the influence of the type and size of the rubber, particle breakage, and damping properties and also account for train-induced cyclic loading in models developed for railway substructures. This paper contributes to advancing future research aimed at deepening the fundamental understanding of rubber-mixed materials used in transportation infrastructure.

Keywords: constitutive modelling; waste materials; recycled rubber; transport infrastructure; stress–strain behaviour

Academic Editors: Antonis A. Zorpas, Paolo Sospiro and Marta Rossi

Received: 12 March 2025
Revised: 23 April 2025
Accepted: 25 April 2025
Published: 28 April 2025

Citation: Qi, Y.; Wijesooriya, K.; Indraratna, B.; Riyad, A.S.M. Constitutive Behaviour of Recycled Rubber-Involved Mixtures for Transportation Infrastructure. *Sustainability* **2025**, *17*, 3956. https://doi.org/10.3390/su17093956

1. Introduction

Roads and railways are the most commonly used modes of public transport due to their convenience and the continuous expansion of road and railway networks. Australia has one of the largest transport networks in the world with 873,573 km of roads; this makes it the 9th largest globally, with a railway network spanning 38,500 km that ranks 7th in the world [1]. However, factors such as population growth, industrial expansion, and urbanization have led to a rising demand for further development and expansion of our transport infrastructure. The growing demand for rail transport has led to higher train speeds and increased loading intensity, which in turn has contributed to track deterioration and more frequent maintenance. Every country spends significant amounts of money on the maintenance and development of their transport infrastructure, which means improving operational efficiency and passenger comfort and mitigating construction and maintenance costs are key priorities [2].

Transport infrastructure currently faces several major challenges. The depletion of natural aggregates such as sand and gravel is a pressing concern for many countries, as high-quality aggregates are becoming increasingly scarce due to stricter environmental regulations [3]. Essential materials that are widely used in road pavements and railway tracks, such as gravel and ballast, are typically produced through quarrying. This involves extracting large quantities of sand, gravel, and other raw materials from the earth, which then destroys habitats, depletes resources, and creates ecological degradation, which disrupts local communities and threatens wildlife. Roads and embankments often experience differential settlement [4–6], while railway tracks face additional challenges such as ballast breakage [7–11], excessive vibration [12–14], mud pumping [15–17], ballast fouling [18,19], and the lateral deflection of rails [20]. Moreover, while railway substructures are frequently subjected to damage from impact loads caused by rail irregularities and flat wheels [21,22], the high speeds of heavier trains cause the ballast and sub-ballast to undergo breakage and degradation after millions of loading cycles. Over time, inadequate lateral confinement leads to the spreading and settlement of ballast and sub-ballast, and ballast degradation occurs as the sharp edges and angular corners of particles break, allowing fine particles to infiltrate between the layers [23]. Furthermore, the growing demand for passenger and freight transport has led to the operation of heavier and faster trains, which increase the dynamic loads that intensify ground vibrations, heighten stress on the track substructure, and accelerate the deterioration of track components [13].

On the other hand, the rapid industrialization in the twenty-first century, particularly in Australia, has led to the accumulation of large volumes of waste by-products such as coal wash, coal tailings, steel furnace slag, demolition waste, fly ash, glass, waste tyres, and plastics. These materials pose serious environmental and socio-economic concerns worldwide because the stockpiles often occupy otherwise useable land in suburban and regional areas. Australia also faces challenges in managing the waste rubber from over 21 million registered vehicles, which generated approximately 537,000 tonnes of end-of-life tyres in 2023–2024. Although recycling and energy recovery processes handle around 66% of this waste, approximately 184,000 tonnes of tyres are still dumped illegally, stockpiled, or disposed of in landfills, posing significant environmental risks, particularly in rural and remote regions [24,25].

As a result, the growing demand for sustainable transport infrastructure has driven the search for more environmentally friendly materials with superior engineering properties. The key approach is to adopt "greener" alternatives to natural aggregates because they will reduce reliance on natural resources, support a circular economy, and promote the environmental sustainability of transport infrastructure [26,27]. Recycled waste materials such as crushed glass (i.e., [28–33]), plastics (i.e., [34–36]), coal mining waste (i.e., [37–44]), steel furnace slag (i.e., [45–48]), fly ash (i.e., [49–51]), and construction demolition waste (i.e., [52,53]) are widely utilised because they reduce reliance on scarce natural resources, divert waste from landfills, and lower carbon footprints better than traditional quarried materials, thus promoting environmental sustainability [53,54].

Among the various waste materials available, rubber stands out because its superior energy absorption and damping capacity enable it to mitigate the impact of repeated loads from trains and moving vehicles. For instance, when scrap rubber is mixed with asphalt, pavements are better able to resist rutting, permanent deformation decreases, and fatigue resistance improves [55,56]. In recent years, researchers have focused on incorporating different types of recycled rubber into railway tracks as they recognise their potential to reduce track deterioration, enhance track stability, and provide an eco-friendly solution that supports a circular economy. Mixing rubber crumbs with ballast and coal mining by-products can create energy-absorbing ballast and capping layers, which reduce track vibrations and ballast degradation [10,57–62]. Recycled tyre cells filled with recycled ballast can be incorporated into capping layers in railway tracks to provide substantial lateral confinement, which in turn enhances track stiffness and its energy-absorbing capacity, thereby reducing particle breakage and ballast settlement [63–65]. Moreover, installing rubber geogrids beneath the ballast layer has proven to reduce impact forces and reduce ballast deformation and degradation [66–68]. Rail pads are placed at the rail–sleeper interface to provide flexibility, prevent direct contact between rails and concrete sleepers, and limit vibrations from passing trains [61,69,70]. Under-sleeper pads (USP) positioned at the sleeper–ballast interface and under-ballast mats (UBM) installed beneath the ballast layer are used to enhance the contact area at the ballast–sub-ballast and ballast–sleeper interfaces, respectively, thereby reducing the concentration of stress and reducing ballast breakage and deformation [71–76]. Figure 1 shows the various positions of rubber inclusions within a ballasted railway track.

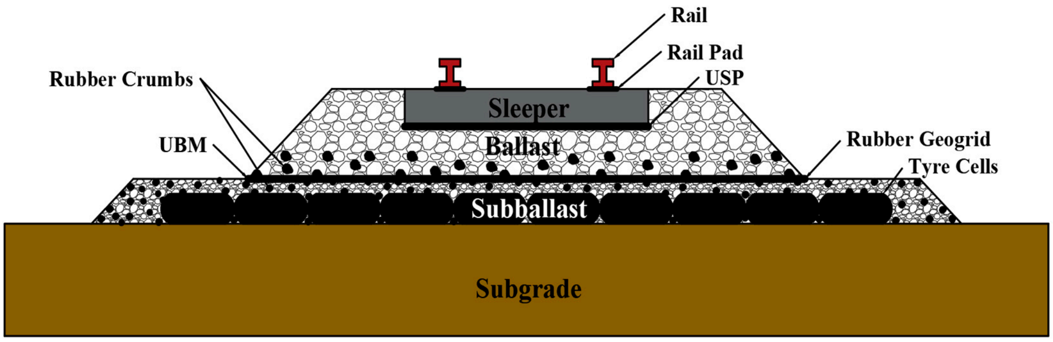

Figure 1. Various rubber inclusions in ballasted tracks across different locations (modified from [69]).

Unlike traditional materials, recycled materials exhibit distinct characteristics that make it imperative to study their fundamental geotechnical behaviour through constitutive relationships [77]. While previous research has investigated the geotechnical properties of waste material mixtures via laboratory experiments, a more comprehensive understanding can be achieved utilizing mathematical approaches. Despite the number of laboratory studies conducted on soil–rubber mixtures, only a limited number have explored their behaviour using theoretical models developed within a constitutive framework, hence the need for further advancements in this area.

Therefore, this paper presents a comprehensive review of the various constitutive models developed to study the behaviour of recycled rubber-involved mixtures for transport infrastructure; this includes sand–rubber mixtures, coal wash–rubber crumb mixtures (CW + RC), and steel furnace slag–coal wash–rubber crumb mixtures (SFS + CW + RC). The effects of adding rubber to these mixtures on the stress–strain behaviour, critical state, shear strength, and dilatancy are critically reviewed, and the advantages and limitations of existing models are elaborated. Additionally, recommendations for future studies are included to address the gaps and unexplored aspects of past research.

2. Stress–Strain Characteristics of Rubber-Mixed Materials

2.1. Stress–Strain Behaviour

Previous studies have investigated the shear behaviour of rubber-mixed granular soils by incorporating different proportions of scrap tyres, measured by weight or volume, and utilizing various test equipment, such as direct shear apparatus and triaxial cells, on dry and fully saturated samples [51,58,78–89]. The stress–strain behaviour of materials mixed with rubber is influenced by the gradation of the material, the confining pressure, the initial void ratio, and the amount of rubber [41,44,90]. Of these, the gravimetric ratio of rubber and confining pressure are the primary factors that govern the shear behaviour of rubber-mixed materials. Indraratna et al. [42] demonstrated that incorporating rubber crumbs into SFS + CW + RC reduces the peak deviator stress because rubber has a lower shear strength than other stiffer components in mixtures like SFS and CW (Figure 2a). However, a higher ratio of SFS to CW compensates for this reduction because SFS provides a greater stiffness. Notably, contraction depends primarily on the amount of rubber: the more rubber, the more constructive the material, while the peak compression strain remains constant when the amount of rubber is the same when comparing SFS + CW + RC with CW + RC mixtures (Figure 2b). When the deviator stress reaches its peak, the mixtures contract and then dilate, while the larger pieces of rubber promote a shift from brittle to ductile behaviour (Figure 2). Similar results were reported by Tawk and Indraratna [58] for CW + RC mixtures used in railway capping layers (Figure 2) and by Arachchige et al. [91] for rubber–ballast mixtures in ballast layers; there, the increasing amount of rubber reduced the peak deviator stress but increased the ductility by raising the axial strain at peak stress. Similar findings for sand–rubber mixtures were reported by Sheikh et al. [86] when they investigated the shear behaviour of rubber crumbs and sand blends using a monotonic triaxial apparatus.

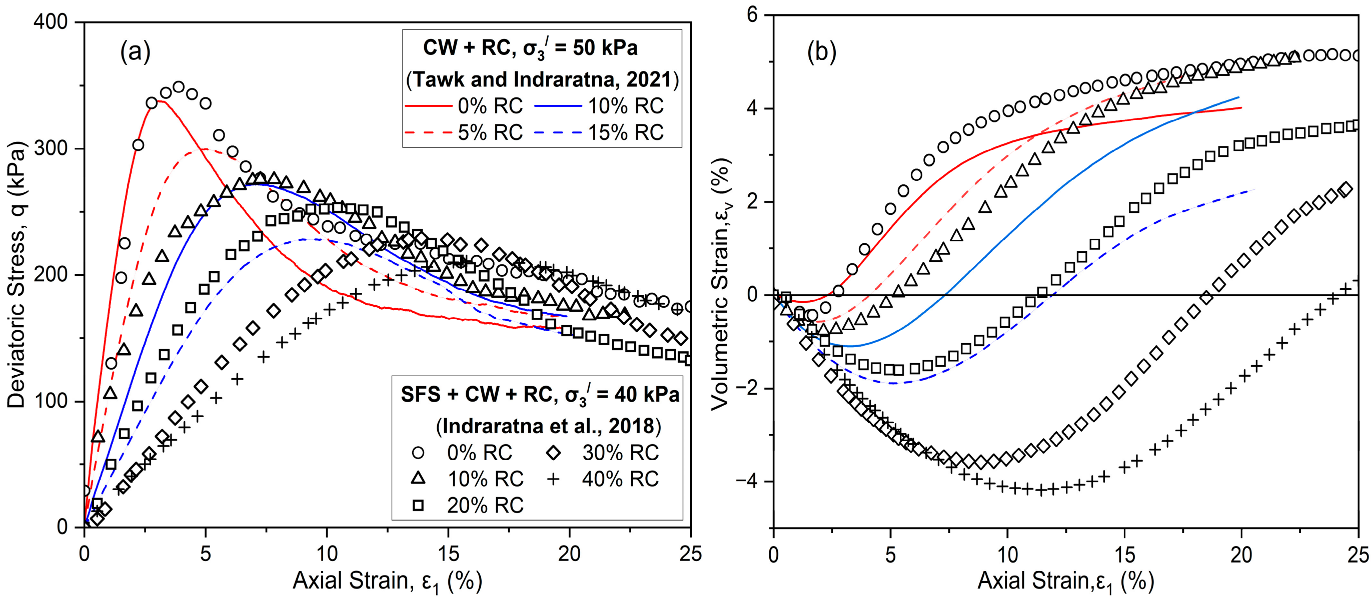

Figure 2. Stress–strain curves of CW + RC and SFS + CW + RC mixtures with varying RC content (**a**) deviator stress-axial strain response and (**b**) volumetric strain-axial strain response (modified from [92], and data sourced from [42,58]).

Studies on mixtures of tyre rubber–sand were initiated in the early 1990s. Ahmed [93] first investigated the shear behaviour of mixtures of sand–tyre chips using static and dynamic triaxial tests. He then analysed the size and ratio of the tyre chips, the type of soil, the confining pressure, and sample preparation. This study concluded that the shear behaviour depends mainly on the amount of tyre chips and the confining pressure. Lee et al. [83] investigated mixtures of rubber–sand with 40% rubber at confining pressures of 28, 97, and 193 kPa for use as lightweight backfill. With this amount of rubber, a clear peak stress could not be seen, even at an axial strain of 25%, thus indicating that the failure strain of these mixtures lies beyond the range of conventional testing equipment. Zornberg et al. [84] noted a similar trend in mixtures of sand–tyre shreds with up to 60% rubber. Lee et al. [83] observed a contractive phase in the volumetric strain followed by dilation at all confining pressures, which is consistent with the observations made by Youwai and Bergado [94] (Figure 3) and Anbazhagan et al. [95]. However, Zornberg et al. [84] only found contraction within the axial strain range for mixtures with less than 60% rubber, whereas adding 60%

rubber caused a shift towards dilative behaviour. Mashiri et al. [85] observed that the deviator stress increased with an increasing amount of tyre chips in the blends of sand–tyre chips, but with more than 20% of chips, it declined slightly (Figure 3). Incorporating tyre chips reduced the dilation of sand, a trend that continued as the amount of chips and the confining pressure increased. Moreover, tyre chips also helped to control post-peak softening and maintain stable dilatancy under various confining pressures.

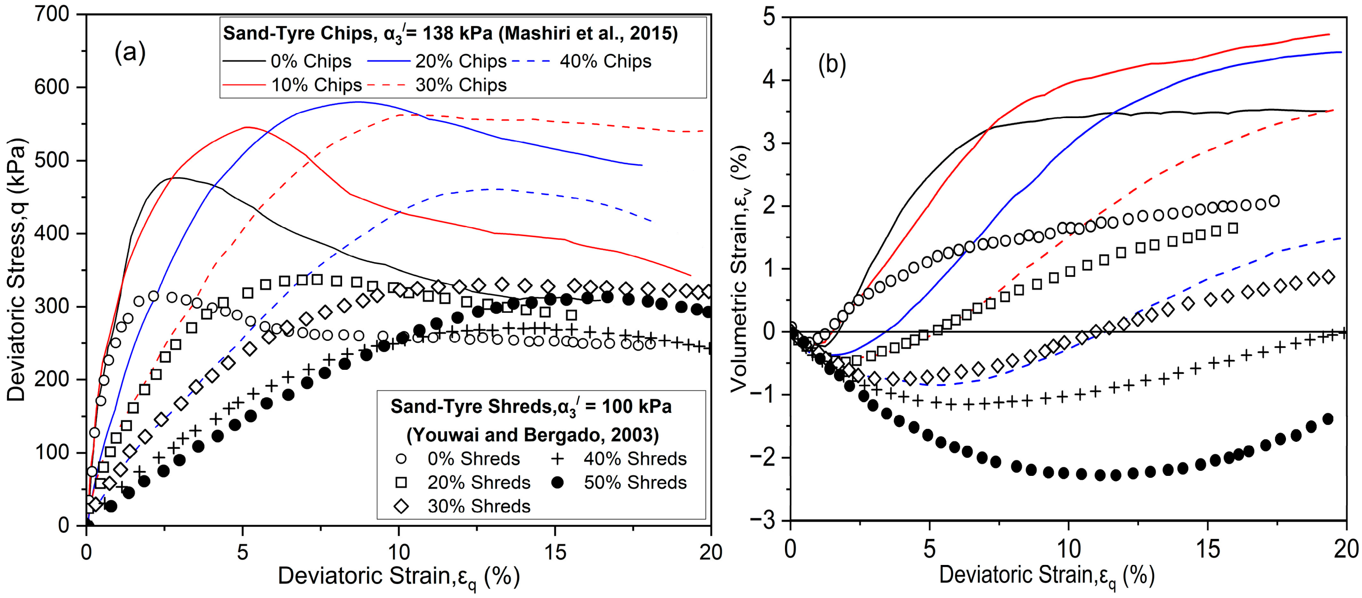

Figure 3. Stress–strain curves of sand–rubber chips and sand–rubber shreds mixtures with varying rubber content (**a**) deviator stress-axial strain response and (**b**) volumetric strain-axial strain response (data from [85,94]).

2.2. Shear Strength

Consistent with the behaviour of other granular materials, mixtures of tyre rubber and soil with a higher confining pressure and relative density were found to exhibit increased shear strength [93]. However, the impact that the amount of rubber had on the shear strength deviated considerably from findings in previous research, as shown in Table 1. Incorporating tyre shreds or chips into sand enhances the shear strength of the mixture [79,80,84,93] mainly due to the increase in the apparent cohesion as the sand and tyre shreds/chips interlock, which is similar to the effect seen in fibre reinforcement [81]. For instance, a study by Edil and Bosscher [80] demonstrated that randomly mixed tyre shreds increased the strength of sand and resulted in a stronger composite. Incorporating 10% of tyre shreds by volume significantly enhanced the strength under low to moderate normal stresses, as reported by Ahmed [93]. The optimal amount of tyre shreds/chips needed to improve the shear strength of the mixtures can vary depending on the source of the materials or the test conditions, as shown in Table 1. However, unlike the observations for sand–rubber chip/shred mixtures, adding tyre crumbs or granulated rubber into sand, ballast, or waste granulates (e.g., CW with or without SFS) actually reduced the shear strength [86,96]. This decrease in the shear strength occurs because the rubber crumbs cannot reinforce the mixture as random shreds/chips do, as observed by Tatlisoz et al. [81], and because in most scenarios, the rubber crumbs are not as strong as the host materials in the mixtures. Figure 4 shows the opposite effect of rubber crumbs and rubber shreds on the shear strength of their mixtures with sand.

Beyond the amount of tyre chips, factors such as the aspect ratio, chip width, normal stress, and the unit weight of the sand matrix may also influence the shear strength of mixtures of sand–tyre chips. However, the effect of particle size ratio on the shear strength of mixtures of sand–rubber shred mixtures is also not consistent. For instance, Lee et al. [97] indicated that the relatively higher size ratio increases its strength. Studies by Ghazavi and Sakhi [82], Zornberg et al. [84], and Rao and Dutta [98] using controlled rectangular-shaped tyre chips with specific dimensions and but varying thicknesses revealed that higher size ratios of tyre chips significantly improved the initial friction angle. On the contrary, Ahmed [93] found that the size of tyre chips had a negligible impact on the shear strength of sand–rubber mixtures.

Table 1. Effect of rubber content on the shear strength of rubber mixed soil.

Effect Type	Reference	Mixtures	Rubber Content (%)	Test/Apparatus	Optimal Rubber Content Considering Shear Strength
Positive effect	Ahmed [93]	Sand–tyre rubber	0–100	Static and dynamic triaxial test	39% by mass
	Edil and Bosscher [80]	Sand–scrap tyre	5, 10, 25	Large-scale direct shear test	10% by volume (5% by mass)
	Tatlisoz et al. [81]	Silty sand–rubber chips/shreds	10, 20, 30	Large-scale direct shear test	At least 30% of rubber chip content
	Foose et al. [79]	Sand–tyre shreds	0, 10, 20, 30	Direct shear test	30% rubber content maximized shear strength
	Zornberg et al. [84]	Sand–tyre shreds	0, 5, 10, 15, 30, 38, 60, 100	Large-scale triaxial test	35% of tyre shreds by mass
	Ghazavi and Sakhi [82]	Sand–rubber shreds	15, 30, 50	Large-scale direct shear test	Friction angle peaks at 50% rubber shreds
	Rao and Dutta [98]	Sand–tyre chips	0, 5, 10, 15, 20, 30, 40, 60, 80, 100	Drained triaxial test; repetitive load test	20% by mass
	Mashiri et al. [85]	Sand–tyre chips	0, 10, 20, 30, 35, 40	Consolidated drained monotonic triaxial	35% by mass
	Anbazhagan et al. [95]	Sand–tyre chips	10, 15, 20, 25, 30, 35	Large-scale direct shear test	30% by volume
	Ahmed et al. [87]	Sand–tyre chips	0, 10, 20, 30, 40	Constant shear-drained stress path	20% by mass
Negative effect	Lee et al. [83]	Sand–tyre chips	40	Consolidated drained triaxial test	Shear strength falls between sand and pure tyre chips
	Youwai and Bergado [94]	Sand–tyre rubber shreds	0, 20, 30, 40, 50, 100%	Isotropic consolidated drained triaxial test	Shear strength decreases as tyre content increases
	Sheikh et al. [86]	Sand–tyre crumbs	0, 10, 20, 30, 40	Static triaxial test	Shear strength decreases as tyre content increases
	Indraratna et al. [42]	CW + SFS + rubber crumbs	0, 10, 20, 30, 40	Monotonic triaxial; drained cyclic triaxial	Shear strength decreases as crumb content increases
	Tawk and Indraratna [58]	CW + rubber crumbs	0, 5, 10, 15	Drained static triaxial	Shear strength decreases as crumb content increases

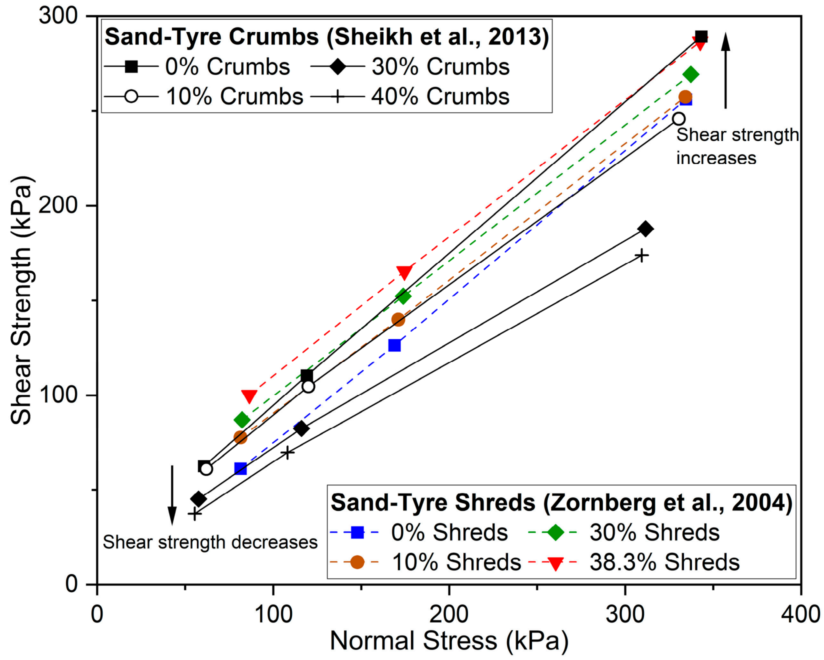

Figure 4. Effect of rubber shreds and crumb inclusion on the shear strength of rubber-mixed sand (data from [84,86]).

3. Constitutive Models for Materials Mixed with Rubber

The number of constitutive models from the literature for aggregates mixed with rubber is quite limited. The few existing ones, including those developed for mixtures of sand–rubber (i.e., [83,94,99–101]), mixtures of CW + RC (i.e., [77]), and mixtures of SFS + CW + RC (i.e., [102]) were developed for monotonic loading conditions inspired by existing models for granular soils, and they are reviewed in the sections below.

3.1. Constitutive Models for Sand–Rubber Mixtures

The first constitutive model for sand–rubber mixtures under monotonic loading for use as a lightweight backfill was proposed by Lee et al. [83], following the hyperbolic model proposed by Duncan et al. [103]. This hyperbolic model concept has also been applied in several other studies to predict the strength and deformation characteristics of sand–rubber blends (i.e., [104]). The relationship between deviatoric stress (q) and axial strain (ε_1) is defined by the hyperbolic function:

$$q = \frac{\varepsilon_1}{\frac{1}{E_i} + \frac{\varepsilon_1}{q_{ult}}} \tag{1}$$

where E_i refers to the initial tangent of Young's modulus, and q_{ult} refers to the asymptotic (ultimate) deviatoric stress that corresponds to the deviatoric stress at failure. The overall dilatancy characteristics cannot be fully captured by hyperbolic models, and neither can the dilative and contractive behaviour. This model can only represent contractive behaviour—it cannot predict the dilative response—and the post-peak strain softening behaviour of rubber–sand mixtures, as shown in Figure 5.

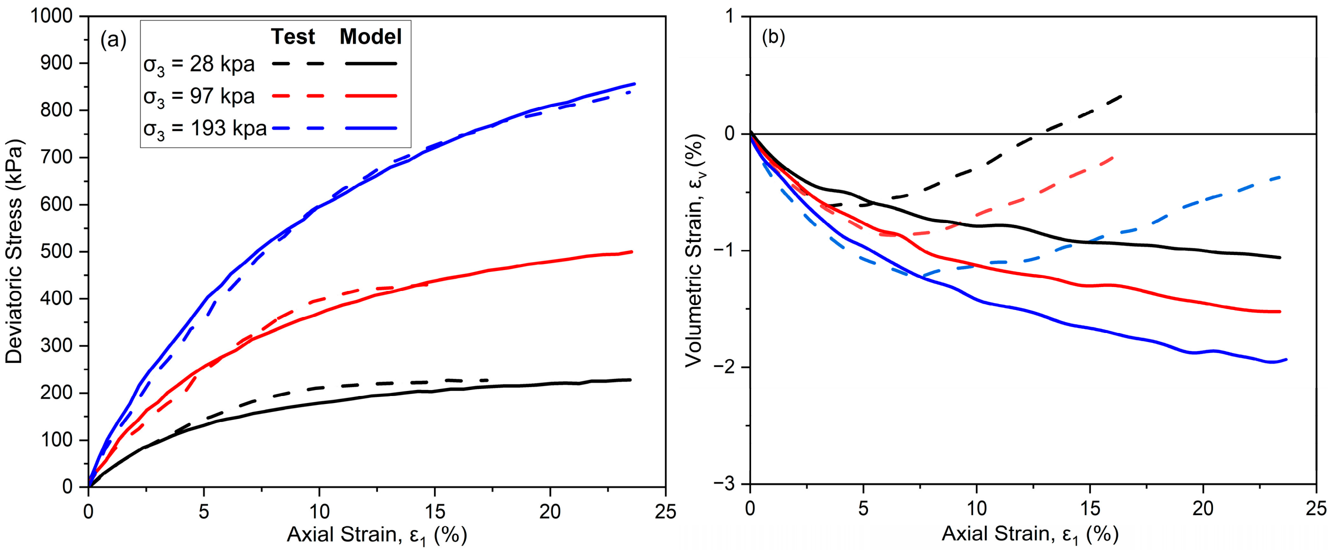

Figure 5. Triaxial compression test results and hyperbolic model predictions for mixtures of rubber and sand: (**a**) deviatoric stress–axial strain curves and (**b**) volumetric strain–axial strain curves (data sourced from [83]).

Youwai and Bergado [94] and Mashiri et al. [99] then modelled the static behaviour of rubber and sand mixtures by utilizing a hypoplasticity model, which captured the overall stress and strain behaviour and the contractive and dilative behaviour, thus addressing the drawbacks of the hyperbolic models. The hypoplastic model presented by Youwai and Bergado [94] is derived from the critical state framework previously developed for sand by Li and Dafalias [105]. The general equations for this model are derived from the plasticity theory introduced by Dafalias [106]:

$$\left\{ \begin{array}{c} \frac{\partial q}{\partial p'} \end{array} \right\} = \left[\begin{pmatrix} 3G & 0 \\ 0 & K \end{pmatrix} - \frac{1}{K_p + 3G - K\eta d} \begin{pmatrix} 9G^2 & -3KG\eta \\ 3KGd & -K^2\eta d \end{pmatrix} \right] \begin{pmatrix} \frac{\partial \varepsilon_s}{\partial \varepsilon_v} \end{pmatrix} \tag{2}$$

where ∂q and $\partial p'$ refer to the increment of deviatoric and mean effective stress, respectively, and G and K are the elastic shear and elastic bulk modulus, respectively. K_P, η, and d denote the plastic modulus, stress ratio, and dilatancy, and $\partial\varepsilon_s$ and$\partial\varepsilon_v$ are the increments of deviator strain and volumetric strain.

The state parameter (ψ), as established by Been and Jefferies [107], was also incorporated to account for state dependence. Meanwhile, Youwai and Bergado [94] observed that the initial dilatancy of mixtures of shredded rubber tyres and sand increased with the mean stress (p), leading to the following modification of the dilatancy equation:

$$d = k_d \left(\frac{p}{p_a}\right)\left(e^{m\psi} - \frac{\eta}{M_{cs}}\right) \tag{3}$$

where k_d and m are the dilatancy parameters, and p_a and M_{CS} denote the atmospheric pressure and critical stress ratio, respectively.

Although this model accurately captures the overall dilatancy, strength, and deformation, determining the accurate critical state for sand and rubber mixtures was difficult because the mixture tended to dilate at large axial strains (25–100%); consequently, the authors assumed that the steady state was reached at 25% strain. In typical granular soils, the critical state is usually achieved after the axial strains exceed 10% [108]. However, for sand–tyre rubber mixtures, reaching a critical state within the strain limit in the laboratory condition proves to be challenging, particularly in mixtures with high tyre content [109].

To address this problem, Disfani et al. [110] allowed the shearing process to continue until an axial strain of approximately 25% was achieved, and this was considered to be the end-of-test state; in their study, this was assumed to represent the critical state. Moreover, Youwai and Bergado [94] confirmed that blends of sand and rubber with the rubber varying from 30% to 100% were unable to reach a fully developed critical state under laboratory conditions. Similarly, it was therefore assumed that the condition at the end of the test was taken as the critical state.

Mashiri et al. [99] presented a semi-empirical constitutive model to capture the monotonic shear behaviour of sand and tyre chip blends based on the critical state framework, plasticity theory, and the state parameter. Since defining the critical state for mixtures of rubber and tyre chips is challenging, the framework was modified into a constant stress ratio approach for the modified hardening and dilatancy functions and the modified state parameter. Shortly after softening, as the dilatancy and increments in the stress ratio decreased, the material reached a constant stress state; thus, the constant stress ratio proposed by Mashiri et al. [85] was used instead of the critical stress ratio. The dilatancy equation developed by Li and Dafalias [105] was adopted by incorporating the hardening parameter and eliminating its dependence on the shear modulus; a new framework was then introduced to identify the model parameters. Mashiri et al. [85] modified the state parameter introduced by Been and Jefferies [107] to quantify the vertical distance between the void ratio (e) of the sand and tyre chip mixture and the constant stress ratio state line (e_{CSR}); this modified state parameter (ψ^*) was adopted in the model as follows:

$$\psi^* = e - e_{CSR} \tag{4}$$

The dilatancy function and the hardening modulus proposed by Li and Dafalias [105] were modified as follows:

$$d = d_0\left(e^{m\psi^*} - \frac{\eta^*}{M^*_{CSR}}\right) \tag{5}$$

$$K^*_p = H^*\left(\frac{M^*_{CSR}}{\eta^*} - e^{m\psi^*}\right) \tag{6}$$

where d_0 is the dilatancy parameters, η^* is the yield stress ratio, M^*_{CSR} is the equivalent stress ratio at constant stress state, K^*_p is the hardening modulus, and H^* is the parameter of the hardening modulus.

This model successfully predicted the hardening and softening of the sand and tyre chip mixture and captured the experimental behaviour of sand mixed with tyres with different amounts of rubber chips. The constant stress ratio is influenced by the relative density of the sand and tyre chip mixtures, but it was not incorporated into the model. Further experimental studies are needed to establish the relationship between the constant stress ratio and relative density.

Cui et al. [101] recently developed an elastoplastic constitutive model within the critical-state framework to predict the dilatancy and stress–strain of sand and rubber with varying amounts of rubber. Cui et al. [101] considered the effect that the amount of rubber would have on the elastic, critical-state, and dilatancy parameters where the amount of rubber by volume (R_V) is a variable. A polynomial function was proposed to count for the nonlinear correlation between those model parameters and the amount of rubber:

$$y = a + bR_v + cR_v^2 \tag{7}$$

where y represents the elastic, critical-state (slope, λ_c and intercept e_Γ of the critical-state line, CSL), and the dilatancy model parameters, and a, b, and c are the fitting parameters.

Figure 6 shows the polynomial relationship of the critical-state parameters changing with the amount of rubber. The influence of the amount of rubber is then incorporated into the model through the state parameter ψ:

$$\psi = e - e_{cs} = e - e_{\Gamma} + \lambda_c \ln p'_{cs} \tag{8}$$

where e_{CS} and p'_{CS} denote the void ratio and effective mean stress (kPa) at the critical state.

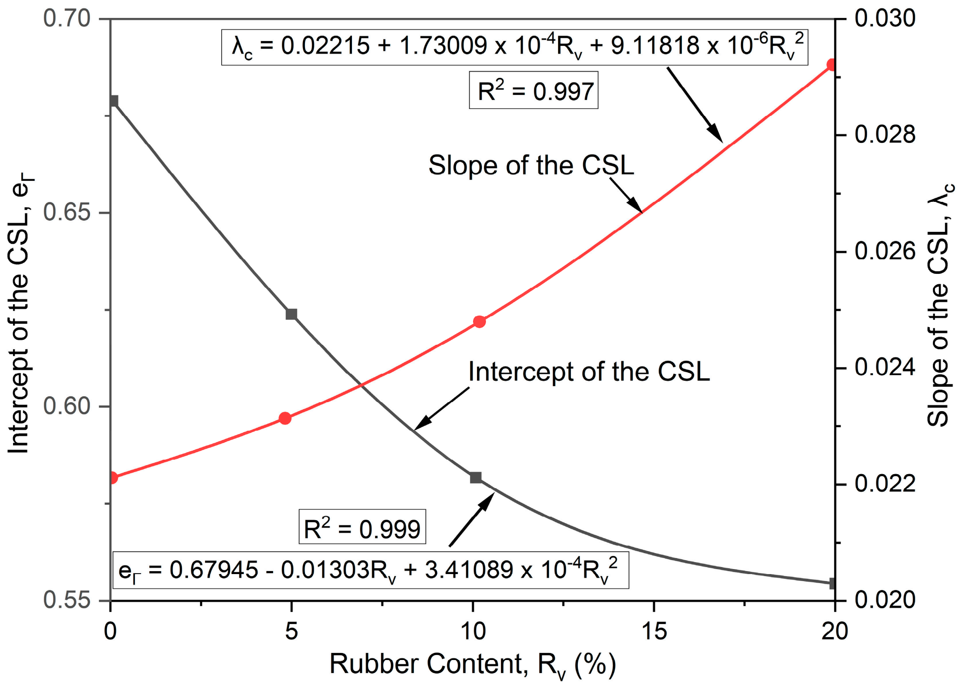

Figure 6. The relationship between the critical-state parameters and the rubber content: e_{Γ} vs. R_V and λ_c vs. R_V (data from [101]).

The dilatancy function was then modified from Li and Dafalias [105] to reflect the dilatancy coefficient of rubber and sand mixtures as follows:

$$d = d_0 \log_{10}\left(e^{m\psi} - \frac{\eta}{M_{cs}} + 1\right) \tag{9}$$

where $\eta = q/p'$ is the stress ratio, while the dilatancy model parameters d_0 and m are defined to fit a polynomial function based on the amount of rubber, and they are expressed as follows:

$$d_0 = 1.79455 - 0.02645R_V + 9.09091 \times 10^{-5}R_V^2 \tag{10}$$

$$m = 1.50055 + 0.02115R_V - 3.09091 \times 10^{-4}R_V^2 \tag{11}$$

In addition, the elastic model parameter G_0 is also defined as a polynomial function of R_V and is expressed as follows:

$$G_0 = 85 - 4.5R_V + 0.1R_V^2 \tag{12}$$

By incorporating these modifications, the model effectively captures the critical-state characteristics, the strain softening behaviour, and the dilatancy characteristics of sand and rubber mixtures. This study further highlights how the confining pressure and amount of rubber influence the peak deviatoric stress, the dilatancy, and the volumetric strain in mixtures of rubber and sand.

In addition to implicit constitutive models utilized to predict the behaviour of rubber and sand mixtures, Li et al. [111] developed an empirical model to determine the maximum dynamic shear modulus of sand and rubber blends by considering the effect of the confining pressure, the size of rubber particle, and the volume of rubber. The maximum shear modulus (G_{dmax}) of a sand and rubber mixture is described in terms of the confining pressure (σ_3) and the rubber content by volume (R_V). G_{dmax} was determined by analysing the experimental data using the multiple regression analysis method below:

$$G_{dmax} = G_1(\alpha_i R_V + \lambda_i)(\theta_i P_a \left(\frac{\sigma_3}{P_a}\right)^{\beta_i}) \tag{13}$$

where G_1 represents the model parameter; α_i, β_i, λ_i, and θ_i are the fitting parameters; and i denotes the size of the rubber particles. P_a also refers to the reference stress, which is considered to be equivalent to the atmospheric pressure. This empirical model accurately represents the attenuation of the shear modulus, which is essential for modelling the dynamic behaviour of sand and rubber mixtures.

3.2. Dilatancy Model for SFS + CW + RC Mixtures

Qi et al. [102] developed a bounding surface model within the critical-state framework for mixtures of steel furnace slag (SFS), coal wash (CW), and rubber crumbs (RC) for railway capping layers, i.e., SFS + CW + RC mixtures. Note that only those mixtures with an optimal mixing ratio of SFS:CW = 7:3 were considered in the model [42,112]. The highlight of this model is that it can capture the energy absorbing property of the mixtures and the influence of the amount of rubber and accurately predict the dilatancy of the mixtures via the semi-empirical relationships of critical-state parameters. Unlike conventional granular materials, the critical-state parameters for SFS+CW+RC mixtures can change with the amount of rubber due to its varying energy absorbing capacity [41,113]. Hence, an empirical relationship was established between the critical-state stress ratio M_{cs}^* and the total work input W_{total} [41], as shown in Figure 7a.

$$M_{cs}^* = M_0 \times \left(\frac{W_{total}}{W_0}\right)^{\alpha} \tag{14}$$

where M_0 is the critical-state ratio if the total work input is equal to 1 kPa, W_0 is the unit work input to ensure the units at both sides of the equation are the same, and α is a material constant that can be obtained through curve regression fitting. The value of M_0 and α is shown in Figure 7a. W_{total} here indicates the total work input when the stress–strain curves reach the peak point, and it can be calculated with the equation below:

$$dW = p' d\varepsilon_v + q d\varepsilon_q \tag{15}$$

where $d\varepsilon_v$ and $d\varepsilon_q$ are the total volumetric and deviatoric strain increments. The critical-state lines for SFS + CW + RC mixtures are linear in the space of $e - \ln p'$, represented by Equation (16), and are found to rotate clockwise as the amount of rubber increases in the mixtures, as seen in Figure 7b. Hence, the parameters Γ^* and λ^* are linked with the dosage of RC by mass, R_b(%):

$$e_{cs} = \Gamma^* - \lambda^* \ln p'_{cs} \tag{16}$$

$$\Gamma^* = \Gamma_1 + \Gamma_2 R_b \tag{17}$$

$$\lambda^* = \lambda_1 + \lambda_2 R_b \tag{18}$$

where $\Gamma_{1,2}$ and $\lambda_{1,2}$ are the regression parameters obtained via Figure 7b, and their values are 0.64, 0.01, 0.069, and 0.003, respectively. By substituting Equations (17) and (18) into

Equation (16), a critical-state surface for the SFS + CW + RC mixtures that change with the amount of RC can be established, as shown in Figure 8:

$$e_{cs} = \Gamma_1 + \Gamma_2 R_b - (\lambda_1 + \lambda_2 R_b)\ln p'_{cs} \quad (19)$$

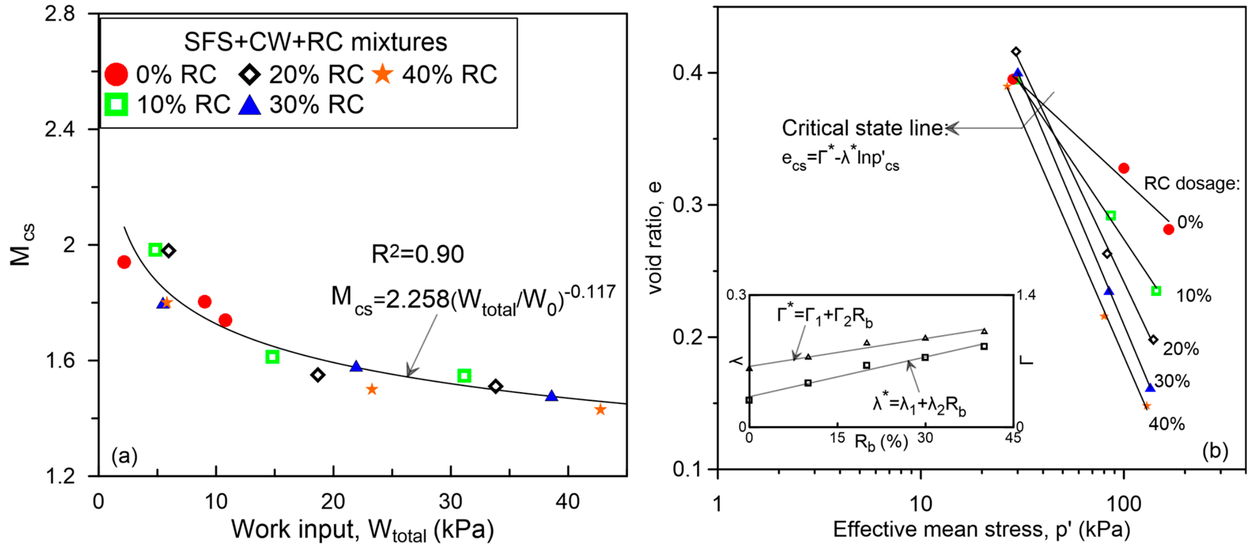

Figure 7. (**a**) The relationship between the critical-state stress ratio and the total work input; (**b**) critical-state lines of SFS+CW+RC mixtures changing with the amounts of RC (modified after [102]).

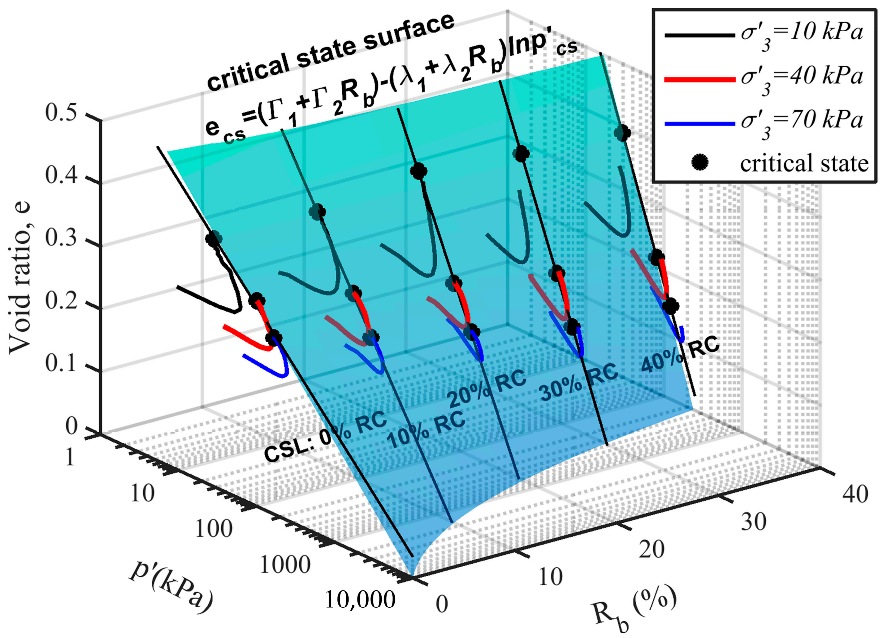

Figure 8. Critical-state surface in the e-lnp′ space with the change in the amount of rubber (after [102] with permission from ASCE).

Therefore, the state parameter $\psi_0 = e - e_{cs}$ is updated to reflect the relationship with the amount of RC:

$$\psi_0 = e - \Gamma_1 + \Gamma_2 R_b - (\lambda_1 + \lambda_2 R_b)\ln p'_{cs} \quad (20)$$

The dilatancy response of the mixtures is calculated following [105] and can be expressed as follows:

$$d = \frac{d\varepsilon_v^p}{d\varepsilon_q^p} = d_0\left(e^{m\psi_0} - \frac{\eta}{M_{cs}^*}\right) \quad (21)$$

where $d\varepsilon_v^p$ and $d\varepsilon_q^p$ are the increments in plastic volumetric and deviatoric strains, respectively. M_{cs}^* and ψ_0 indicate the modified critical-state stress ratio and state parameter as they relate to the total work input and amount of RC represented by Equation (14) and Equation (20), respectively. Figure 9 is a comparison between the experimental data and the model prediction, and this comparison indicates a very good match.

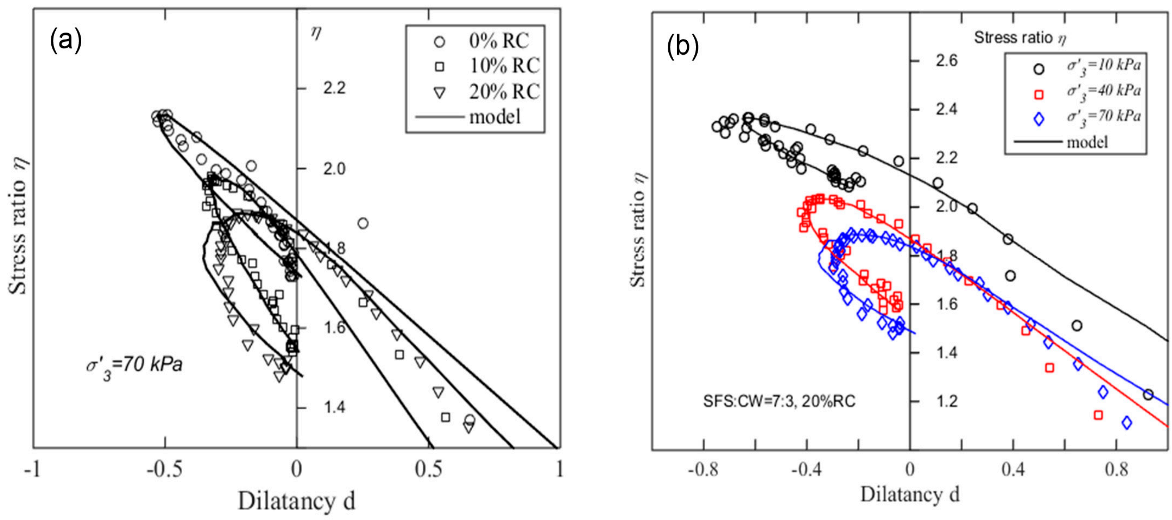

Figure 9. Dilatancy model prediction compared with the experimental data for SFS + CW + RC mixtures with, (**a**) different amounts of RC under a confining pressure of 70 kPa, and (**b**) with 20% of RC under a different confining pressure (modified after [41]).

3.3. Constitutive Model for CW + RC Mixtures

Riyad et al. [77] developed a new constitutive model for waste granular mixtures for railway capping layers based on the bounding surface concept, it includes a modified void ratio (e*) to better capture the compressibility of rubber. Experimental data from consolidated drained triaxial tests on mixtures of coal wash and rubber crumbs (CW+RC) with varying rubber crumbs contents by mass (R_b), as reported by Indraratna et al. [114] was utilised to calibrate and validate the model.

Inspired by Jefferies and Been [115], this study considered a bullet-shaped bounding surface that encompasses the triaxial compression part. The shape of the bounding surface is assumed to be identical to the loading surface, i.e., where the bounding surface $F_b\left(\overline{p'}, \overline{q}, \overline{p'_c}\right) = 0$ and for the loading surface $f_L(p', q, p'_c) = 0$ are in densely compacted conditions (Figure 10).

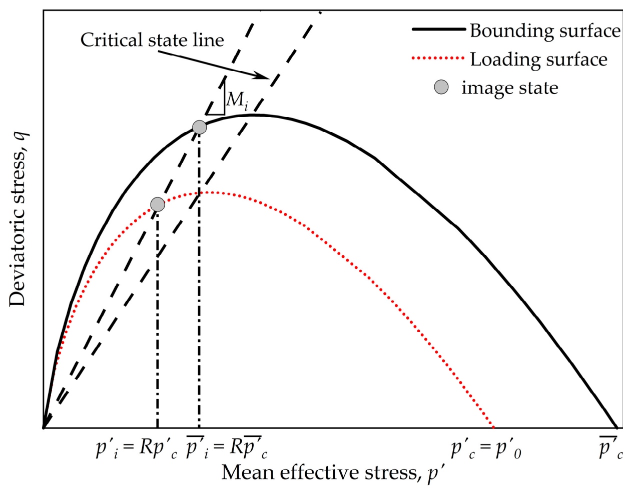

Figure 10. Loading surface and bounding surface in the q-p′ plane (modified after [77]).

The bounding surface and the loading surface are defined as shown in Equation (22) and Equation (23) [77].

$$F_b\left(\overline{p'}, \overline{q}, \overline{p'_c}\right) = \left\{ \overline{q} - (M_{cs} + N\psi_i\chi_i)\overline{p'}\left[1 + \ln\left(\frac{R\overline{p'_c}}{\overline{p'}}\right)\right]\right\} = 0, \text{ for } \psi_i < 0 \tag{22}$$

$$f_L\left(p', q, p'_c\right) = \left\{ q - (M_{cs} + N\psi_i\chi_i)p'\left[1 + \ln\left(\frac{Rp'_c}{p'}\right)\right]\right\} = 0, \text{ for } \psi_i < 0 \tag{23}$$

$$\text{where } \overline{p'_c} = \frac{p_r}{R}\exp\left(\frac{\Gamma - e^* - \kappa \ln p'}{\lambda - k}\right) \tag{24}$$

$$e^* = \left\{e_0 + \varepsilon_v^*(1 + e_0)\right\}\left(1 + \frac{R_b}{100} \times \frac{G_{s,CW}}{G_{s,RC}}\right) \tag{25}$$

$$\psi_i = e^* - e_{cs,i} \tag{26}$$

where p'_c and $\overline{p'_c}$ represents the intercept between the loading and bounding surfaces with the q = 0 axis, respectively (Figure 10). The stress ratio at the image state $(M_{cs} + N\psi_i\chi_i)$ is denoted as M_i in Figure 10. The material constant R relates the intercepts of the bounding and loading surfaces with the M_i line. p_r is a reference stress (typically 1 kPa) used for dimensional consistency. λ and κ are the gradients of the critical-state void ratio and swelling lines. Γ is the void ratio at p_r, and ψ_i represents the state parameter at the image state. e* is the modified void ratio, which incorporates the change in volume of the rubber crumbs. $G_{S,CW}$ and $G_{S,RC}$ are the specific gravities of coal wash and rubber crumbs, respectively. ε_v^* is the void volumetric strain and only accounts for the change in volume of stiff particles (i.e., CW). N is the volumetric coupling parameter, which is proposed to lessen the effect of dilatancy on the shear strength, inspired by Nova and Wood [116], as expressed in the below equation:

$$\eta = (N - 1)D^p + M_{cs} \tag{27}$$

$D^p = \frac{d\varepsilon_v^p}{d\varepsilon_q^p}$ is the plastic dilatancy. The dilatancy at the peak deviator stress D^p_{peak} is typically linear and correlated with the state parameter at the peak deviator stress $\psi_{\eta max}$ [77]. Since there is no elastic strain at peak stress, $D^p_{peak} = D_{peak}$.

$$D_{peak} = D^p_{peak} = \chi\psi_{\eta max} \tag{28}$$

where χ is the dilatancy constant at the image state condition and is given by Equation (26):

$$\chi_i = \frac{\chi M_{cs}}{M_{cs} - \lambda\chi} \tag{29}$$

The plastic dilatancy D^p is related to the plastic potential and is obtained by substituting Equation (27) into Equation (22):

$$D^p = M_i \ln\left(\frac{\overline{p'}}{R\overline{p'_c}}\right) \tag{30}$$

The hardening rule in this study is expressed mathematically by Equation (31):

$$\frac{d\left(R\overline{p'_c}\right)}{R\overline{p'_c}} = H \times \left(\frac{R\overline{p'_c}}{\overline{p'}}\right)^{-2} \times \left(\left(\overline{p'_c}\right)_{max} - \overline{p'_c}\right) \times \frac{d\varepsilon_q^p}{\overline{p'_c}} \tag{31}$$

$$H = H_{min}\left(\sigma_3'\right)^{-\beta}\exp(-\delta_H R_b) \quad (32)$$

where H_{min} is the minimum hardening modulus at p_r, β relates to changes in the confining pressure (σ_3'), and δ_H denotes the diminution of H with the amount of rubber.

Figure 11 shows the predicted stress–strain and volumetric strain curves for CW + RC mixtures; they match the test data from [114]. The model thus accurately captures the overall volumetric response and stress–strain relationship, with strain hardening and the peak deviator stress increasing with the confining pressure. As the amount of rubber increases, the peak deviator stress decreases, and strain softening shifts to strain hardening; this indicates a transition from brittle to ductile behaviour.

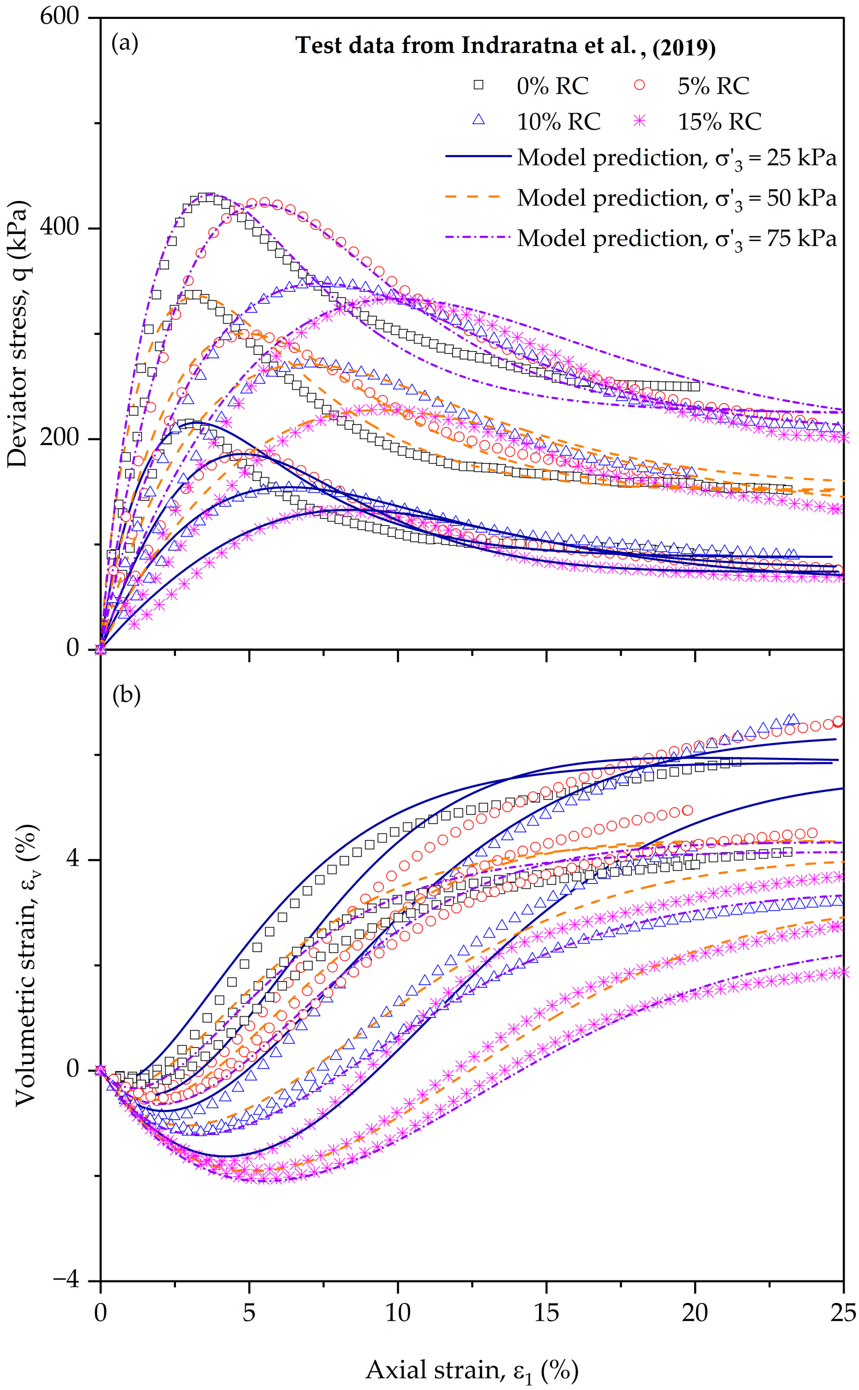

Figure 11. Test results and model prediction for CW + RC mixtures with varying amounts of rubber and confining pressures; (**a**) is the deviator stress, and (**b**) is the volumetric strain (modified after [77], and data sourced from [114]).

4. Model Limitations and Applications

Table 2 provides a summary of the highlights and limitations of the aforementioned constitutive models. In addition to the inherent limitations of the model itself, as outlined in Table 2, most existing models (with the exception of Riyad et al. [77]) do not account for the deformable nature of rubber, which is a key characteristic that should be incorporated into future research. Moreover, more complex conditions, such as cyclic loading and unsaturated conditions that have yet to be addressed in current models, should also be considered.

Table 2. Highlights and limitations of the constitutive models for rubber-mixed materials.

References	Mixtures	Model Concepts	Highlights	Limitations
Lee et al. [83]	Sand–rubber crumbs	Hyperbolic model	A simple model to capture the strain hardening response of sand–rubber mixtures	Cannot capture the strain-softening response and the dilative behaviour
Youwai and Bergado [94]	Sand–rubber shreds	Hypoplastic model; critical-state framework	Assumed that the condition at the end of the test was taken as the critical state	Could not determine the accurate critical-state parameters
Mashiri et al. [99]	Sand–rubber chips	Hypoplastic model; critical-state framework	Developed the constant stress ratio to replace the critical state ratio	The constant stress ratio cannot exactly represent the critical-state ratio; hence, it still induces the divergence between the model prediction and test results
Cui et al. [101]	Sand–rubber crumbs	Elastoplastic constitutive model; critical-state framework	Established polynomial functions to incorporate the influence of rubber on the elastic, critical state, and dilatancy parameters	A lot of curve-fitting relationships may not be suitable for other rubber-mixed materials
Li et al. [111]	Sand-rubber crumbs	Empirical model	Developed an exponential relationship between the maximum shear modulus and the rubber content by volume and confining pressures	Concerning only the maximum shear modulus rather than the stress–strain relationship
Qi et al. [102]	Steel furnace slag–coal wash–rubber crumbs	Bounding surface model; critical-state framework	Extrapolation methods were used to determine the critical state; developed a relationship of energy with the critical-state ratio; modified critical-state and dilatancy parameters with the confining pressures and rubber contents	The influence of particle breakage of coal wash and the deformation of rubber particles was not considered
Riyad et al. [77]	Coal wash–rubber crumbs	Bounding surface model; critical-state framework	Used the revised void ratio to incorporate the deformation of rubber particles	The energy absorbing property of rubber and the breakage of coal wash were not considered

It is noteworthy that in all the hypoplastic, elastoplastic, and bounding surface models developed for rubber-mixed materials, the critical-state framework has been consistently adopted. The primary focus of these models has been on modifying the critical-state parameters and determining the critical state. This emphasis stems from the fact that rubber significantly enhances the ductility of the mixtures, which in turn can delay the occurrence of the critical state in the mixtures having small rubber particles or make it more challenging to achieve for the mixtures having larger tyre chips or shreds. The impact of rubber on the critical state varies with the type of host material and rubber particle size, leading to diverse modifications in the critical-state parameters. Consequently, the methods for identifying the critical state also differ depending on the rubber content and rubber size. For instance, a constant stress state or the end-of-the-test state has been considered as the critical state for sand–rubber chips/shreds mixtures [94,99], while extrapolation was used for SFS + CW + RC mixtures having 20–40% rubber by mass [102].

Although the hyperbolic model has seldom been used for rubber-modified materials since Lee et al. [83], it remains a promising approach for loosely packed rubber-mixed materials, as it effectively captures the behaviour of strain hardening. For mixtures containing rubber chips or shreds, the hypoplastic models [94,99] may be more appropriate, as they offer a viable alternative to the critical-state parameters, particularly where the critical state cannot be defined due to the continuous deformation associated with the larger rubber particle sizes. While the elastoplastic constitutive model [101] serves as an excellent reference for sand–rubber mixtures, it should be applied with caution to other rubber-modified materials, as the fitted relationships may not hold due to variations in material composition. Similarly, the bounding surface models [77,102] developed for the mixtures of coal wash–rubber with or without steel furnace slag show strong predictive performance and may be extended to other rubber–waste mixtures with confidence. Finally, the experimental model for maximum shear modulus [111] presents a valuable reference point for developing constitutive models under dynamic loading conditions, contributing to a more accurate representation of rubber-mixed materials in such scenarios.

5. Conclusions and Recommendations

This paper reviews the existing constitutive models developed for materials mixed with rubber, i.e., sand mixed with rubber, mixtures of steel furnace slag–coal wash–rubber crumbs (SFS + CW + RC), and mixtures of coal wash and rubber crumbs (CW + RC). The key findings of this study are outlined below:

- The shear behaviour of rubber and granular mixtures is primarily governed by the confining pressure and the amount of (shredded) rubber tyres. The inclusion of rubber in granular soil mixtures significantly influences the stress–strain response, improves its energy absorption ability, increases its ductility, and reduces its dilative behaviour. Moreover, the shear strength of materials mixed with rubber depends on the type and amount of rubber and the confining pressure. While including rubber shreds and chips in the mixtures enhances the shear strength through particle interlocking, the addition of rubber crumbs tends to reduce the shear strength due to its lack of structural reinforcement;
- The constitutive models developed for mixtures of sand and rubber lightweight backfill material highlight the significant advancements in predicting stress–strain behaviour. The early hyperbolic model struggled with post-peak softening and dilatancy. To overcome these limitations, the hypoplastic model was developed by incorporating state-dependent behaviour to enable the prediction of dilative and compressive behaviour. Critical state and bounding surface plasticity models further refined these predictions by accounting for variations in the amount of rubber and capturing the hardening and softening in mixtures of sand and rubber. An empirical model was also developed to estimate the dynamic shear modulus;
- The dilatancy model developed for mixtures of SFS + CW + RC to be used as a railway capping layer within the critical-state framework also captured the energy absorbing properties of the mixture due to inclusion of rubber and its influence on dilatancy behaviour. Unlike conventional granular materials the critical-state parameters varied with the amount of rubber due to changes in its energy absorption

capacity. The predicted stress–strain behaviour of the mixture aligned well with the laboratory observations;

- The constitutive model for mixtures of CW + RC predicted the stress–strain behaviour of mining waste and rubber crumbs using a bounding surface plasticity approach with a compressibility-dependent void ratio to consider the effect of rubber inclusion on the volumetric deformation of the mixture and an image of the critical state. An image-state ratio-based plastic flow rule and a hardening modulus that depends on the amount of rubber and the confining pressure were used to model the stress–strain behaviour. The model remains suitable for capping layers involved with rubber particles, though further refinements are needed to better account for the internal deformation of rubber within the granular matrix.

Existing constitutive models for waste materials mixed with rubber were developed primarily for static loading, whereas the railway capping layers experience train-induced cyclic loading. Future models should capture the cyclic behaviour by incorporating energy absorbed by the rubber through its deformation, the reduced particle breakage of the host materials (e.g., sand, CW, etc.), damping effects, and evolving fabric arrangement under loading (e.g., how the skeleton changes with increasing rubber contents or upon deformation under various loading conditions). Furthermore, the effect of the size and type of rubber (e.g., rubber crumbs, rubber fibre, or rubber chips) should be considered when developing models to ensure more accurate predictions of material behaviour. Finally, while rubber is used in pavements, its mechanical behaviour lacks mathematical analysis (e.g., long-term stress–strain response under repeated loading), which is why developing constitutive models for pavements modified by rubber is essential to predict their performance and optimise their design.

Author Contributions: Conceptualization, Y.Q.; methodology, Y.Q. and B.I.; validation, Y.Q., K.W. and A.S.M.R.; formal analysis, Y.Q., K.W., B.I. and A.S.M.R.; investigation, Y.Q., K.W., B.I. and A.S.M.R.; resources, B.I. and Y.Q.; data curation, Y.Q., K.W., B.I. and A.S.M.R.; writing—original draft preparation, Y.Q., K.W. and A.S.M.R.; writing—review and editing, Y.Q., K.W., B.I. and A.S.M.R.; visualization, Y.Q.; supervision, B.I. and Y.Q.; funding acquisition, B.I. and Y.Q. All authors have read and agreed to the published version of the manuscript.

Funding: This research was funded by the Australian Research Council Discovery Project (ARCDP220102862) and Linkage Project (LP200200915). Significant financial support from Sydney Trains, Transport for NSW, SMEC, Bently Systems, Bestech Australia, and other industry organizations over the years is gratefully appreciated.

Data Availability Statement: The data presented in this study are openly available in the references cited by the Tables or Figures.

Acknowledgments: The authors would like to acknowledge the financial support from the Australian Research Council for ARCLP200200915 and ARCDP220102862. The authors would also like to express appreciation for the technical and financial support from industry partners, including Sydney Trains, Bentley Systems Pty. Limited, SMEC Australia Pty. Limited, and Bestech Australia Pty. Limited. Some figures were reproduced from the authors' past publications published in *Acta Geotechnica*, *Geo-congress2020* and *The International Journal of Geomechanics* with kind permissions from Springer and ASCE.

Conflicts of Interest: The authors declare no conflicts of interest.

Abbreviations

CSL	Critical-state line
CSR	Constant stress ratio
CW	Coal wash
RC	Rubber crumbs
SFS	Steel furnace slags
UBM	Under-ballast mats
USP	Under-sleeper pads
a, b, c	Curve-fitting parameters
d	Dilatancy
d_0, k_d, m	Dilatancy parameters
D^p	Plastic dilatancy
D^p_{peak}	Plastic dilatancy at the peak deviator stress
e, e*	Void ratio, modified void ratio
e_{CS}	Void ratio at the critical state
e_Γ	Intercept of the CSL
E_i	Initial tangent of Young's modulus
G	Elastic shear modulus
G_0	Elastic model parameter
G_{dmax}	Maximum shear modulus
$G_{S,CW}$, $G_{S,RC}$	Specific gravities of CW and RC
H_{min}	Minimum hardening modulus at p_r
H*	Hardening modulus parameter
K	Elastic bulk modulus
K_P	Plastic modulus
K^*_p	Hardening modulus
M_{CS}, M^*_{cs}	Critical-state stress ratio, modified critical-state stress ratio
M^*_{CSR}	Equivalent stress ratio at the constant stress state
M_0	Critical-state ratio when total work input is equal to 1 kPa
N	Volumetric coupling parameter
p, p′	Mean stress, effective mean stress
p_a	Atmospheric pressure
p_r	Reference stress (=1 kPa)
p'_{CS}	Effective mean stress at the critical state
p'_c, $\overline{p'_c}$	Intercept between the loading surface and bounding surface with the q = 0 axis
q, q_{ult}	Deviatoric stress, ultimate deviatoric stress
R	Material constant
R_b, R_V	Rubber content by mass and rubber content by volume
W_{total}	Total work input
W_0	Unit work input
α	Material constants
α_i, β_i, λ_i, θ_i	Curve-fitting parameters
δ_H	Diminution of H with the amount of rubber
ε_1, ε_q, ε_v	Axial strain, deviatoric strain, volumetric strain
$\partial\varepsilon_s$, $\partial\varepsilon_v$	Increments of deviator, volumetric strain
$d\varepsilon_q$, $d\varepsilon_v$	Increments of total deviatoric, total volumetric strain
$d\varepsilon^p_q$, $d\varepsilon^p_v$	Increments in plastic deviatoric, plastic volumetric strain
ε^*_v	Void volumetric strain
Γ	Void ratio at p_r
Γ*	Modified void ratio at p'_{CS} = 1 kPa
Γ_1, Γ_2	Calibration parameters for Γ^*
η, *	Stress ratio, yield stress ratio
κ	Gradient of the swelling line

λ	Gradient of the critical-state void ratio line
λ_c	Slope of the critical-state line
λ^*	Gradient of the modified critical-state line
λ_1, λ_2	Calibration parameters for λ^*
ψ, ψ^*, ψ_i	State parameter, modified state parameter, state parameter at the image state
χ	Dilatancy constant at the image state condition
σ_3'	Effective confining pressure
∂q	Increment of deviatoric stress
$\partial p'$	Increment of mean effective stress

References

1. Gharehbaghi, K.; McManus, K.; Robson, K.; Paterno, D.; Myers, M. High-speed rail transportation: Key factors for the Australian eastern states. *World Rev. Intermodal Transp. Res.* **2020**, *9*, 174–197. [CrossRef]
2. Zhai, W.; Wei, K.; Song, X.; Shao, M. Experimental investigation into ground vibrations induced by very high-speed trains on a non-ballasted track. *Soil Dyn. Earthq. Eng.* **2015**, *72*, 24–36. [CrossRef]
3. Qi, Y.; Indraratna, B.; Ngo, T.; Arachchige, C.M.K.; Hettiyahandi, S. Sustainable solutions for railway using recycled rubber. *Transp. Geotech.* **2024**, *46*, 101256. [CrossRef]
4. Kim, M.; Tutumluer, E.; Kwon, J. Nonlinear Pavement Foundation Modeling for Three-Dimensional Finite-Element Analysis of Flexible Pavements. *Int. J. Geomech.* **2009**, *9*, 195–208. [CrossRef]
5. Kodikara, J.; Islam, T.; Sounthararajah, A. Review of soil compaction: History and recent developments. *Transp. Geotech.* **2018**, *17*, 24–34. [CrossRef]
6. Liu, L.; Li, Z.; Cai, G.; Geng, X.; Dai, B. Performance and prediction of long-term settlement in road embankments constructed with recycled construction and demolition waste. *Acta Geotech.* **2022**, *17*, 4069–4093. [CrossRef]
7. Indraratna, B.; Salim, W. Deformation and Degradation Mechanics of Recycled Ballast Stabilised with Geosynthetics. *Soils Found.* **2003**, *43*, 35–46. [CrossRef]
8. Zhao, C.; Xie, Z.; Yu, F.; Zhu, C.; Bian, X.; Chen, Y. Breakage characteristics of ballast particle in uniaxial compression tests incorporating shape and size effects. *Constr. Build. Mater.* **2024**, *447*, 138155. [CrossRef]
9. Indraratna, B.; Lackenby, J.; Christie, D. Effect of confining pressure on the degradation of ballast under cyclic loading. *Géotechnique* **2005**, *55*, 325–328. [CrossRef]
10. Arachchige, C.M.K.; Indraratna, B.; Qi, Y.; Vinod, J.S.; Rujikiatkamjorn, C. Deformation and degradation behaviour of Rubber Intermixed Ballast System under cyclic loading. *Eng. Geol.* **2022**, *307*, 106786. [CrossRef]
11. Wong, C.P.Y.; Coop, M.R. The contact mechanics of a UK railway ballast. *Géotechnique* **2023**, *74*, 1700–1712. [CrossRef]
12. Zhai, W.M.; Wang, K.Y.; Lin, J.H. Modelling and experiment of railway ballast vibrations. *J. Sound Vib.* **2004**, *270*, 673–683. [CrossRef]
13. Qi, Y.; Indraratna, B. Influence of Rubber Inclusion on the Dynamic Response of Rail Track. *J. Mater. Civ. Eng.* **2022**, *34*, 04021432. [CrossRef]
14. Milne, D.R.M.; Le Pen, L.M.; Thompson, D.J.; Powrie, W. Properties of train load frequencies and their applications. *J. Sound Vib.* **2017**, *397*, 123–140. [CrossRef]
15. Nguyen, T.; Indraratna, B.; Kelly, R.; Phan, N.M.; Haryono, F. Mud pumping under rail tracks: Mechanisms, Assessments, and solutions. *Aust. Geomech. J.* **2019**, *54*, 59–80.
16. Bian, X.; Wan, Z.; Zhao, C.; Cui, Y.; Chen, Y. Mud pumping in the roadbed of ballastless high-speed railway. *Géotechnique* **2023**, *73*, 614–628. [CrossRef]
17. Indraratna, B.; Singh, M.; Nguyen, T. The mechanism and effects of subgrade fluidisation under ballasted railway tracks. *Railw. Eng. Sci.* **2020**, *28*, 113–128. [CrossRef]
18. Tennakoon, N.; Indraratna, B.; Rujikiatkamjorn, C.; Nimbalkar, S.; Neville, T. The Role of Ballast Fouling Characteristics on the Drainage Capacity of Rail Substructure. *Geotech. Test. J.* **2012**, *35*, 629–640. [CrossRef]
19. Nimbalkar, S.S.; Tennakoon, N.; Indraratna, B. Effects of Fouling and Degradation on Geotechnical Behaviour of Railway Ballast. In Proceedings of the Indian Geotechnical Conference (IGC 2015): Geotechnics for Infrastructure and Foundation Techniques (GIFT), Pune, India, 17–19 December 2015.
20. Le Pen, L.M.; Powrie, W. Contribution of Base, Crib, and Shoulder Ballast to the Lateral Sliding Resistance of Railway Track: A Geotechnical Perspective. *Proc. Inst. Mech. Engineers. Part F J. Rail Rapid Transit* **2011**, *225*, 113–128. [CrossRef]
21. Vale, C. Wheel Flats in the Dynamic Behavior of Ballasted and Slab Railway Tracks. *Appl. Sci.* **2021**, *11*, 7127. [CrossRef]
22. Sattari, S.; Saadat, M.; Mirtalaie, S.H.; Salehi, M.; Soleimani, A. Effects of train speed, track irregularities, and wheel flat on wheel-rail dynamic forces. *Int. J. Heavy Veh. Syst.* **2023**, *30*, 734–751. [CrossRef]

23. Indraratna, B.; Qi, Y.; Ngo, T.N.; Rujikiatkamjorn, C.; Neville, T.; Ferreira, F.B.; Shahkolahi, A. Use of Geogrids and Recycled Rubber in Railroad Infrastructure for Enhanced Performance. *Geosciences* **2019**, *9*, 30. [CrossRef]
24. Afrin, H.; Huda, N.; Abbasi, R. Study on End-of-Life Tires (ELTs) Recycling Strategy and Applications. *IOP Conf. Ser. Mater. Sci. Eng.* **2021**, *1200*, 12009. [CrossRef]
25. Tyre Stewardship Australia. Australian Tyre Consumption and Recovery 2023–2024. Australian Government Accredited Product Stewardship Scheme. 2025. Available online: https://www.tyrestewardship.org.au/wp-content/uploads/2025/01/Australian-Tyre-Consumption-and-Recovery-2023-24.pdf (accessed on 11 March 2025).
26. Indraratna, B.; Qi, Y.; Ngo, T.; Malisetty, R.; Arachchige, C.K. Innovative and cost-effective rail track construction using recycled rubber. *Railw. Eng. Sci.* **2024**. [CrossRef]
27. Indraratna, B.; Qi, Y.; Rujikiatkamjorn, C. *Waste Materials Utilisation for Transport Infrastructure*, 1st ed.; Taylor & Francis Group: Milton, ON, Canada, 2025.
28. Naeini, M.; Mohammadinia, A.; Arulrajah, A.; Horpibulsuk, S. Recycled Glass Blends with Recycled Concrete Aggregates in Sustainable Railway Geotechnics. *Sustainability* **2021**, *13*, 2463. [CrossRef]
29. Mohajerani, A.; Vajna, J.; Cheung, T.H.H.; Kurmus, H.; Arulrajah, A.; Horpibulsuk, S. Practical recycling applications of crushed waste glass in construction materials: A review. *Constr. Build. Mater.* **2017**, *156*, 443–467. [CrossRef]
30. Arulrajah, A.; Ali, M.; Disfani, M. Recycled-Glass Blends in Pavement Base/Subbase Applications: Laboratory and Field Evaluation. *J. Mater. Civ. Eng.* **2013**, *26*, 04014025. [CrossRef]
31. Perera, S.T.A.; Saberian, M.; Zhu, J.; Roychand, R.; Li, J. Effect of crushed glass on the mechanical and microstructural behavior of highly expansive clay subgrade. *Case Stud. Constr. Mater.* **2022**, *17*, e01244. [CrossRef]
32. Disfani, M.M.; Arulrajah, A.; Bo, M.W.; Hankour, R. Recycled crushed glass in road work applications. *Waste Manag. (Elmsford)* **2011**, *31*, 2341–2351. [CrossRef]
33. Arulrajah, A.; Ali, M.M.Y.; Disfani, M.M.; Piratheepan, J. *Suitability of Using Recycled Glass-Crushed Rock Blends for Pavement Subbase Applications*; ASCE: Reston, VA, USA, 2011; pp. 1325–1334.
34. Arulrajah, A.; Yaghoubi, E.; Wong, Y.C.; Horpibulsuk, S. Recycled plastic granules and demolition wastes as construction materials: Resilient moduli and strength characteristics. *Constr. Build. Mater.* **2017**, *147*, 639–647. [CrossRef]
35. Hasheminezhad, A.; Farina, A.; Yang, B.; Ceylan, H.; Kim, S.; Tutumluer, E.; Cetin, B. The utilization of recycled plastics in the transportation infrastructure systems: A comprehensive review. *Constr. Build. Mater.* **2024**, *411*, 134448. [CrossRef]
36. Peddaiah, S.; Burman, A.; Sreedeep, S. Experimental Study on Effect of Waste Plastic Bottle Strips in Soil Improvement. *Geotech. Geol. Eng.* **2018**, *36*, 2907–2920. [CrossRef]
37. Kaliboullah, C.I.; Indraratna, B.; Heitor, A.; Rujikiatkamjorn, C. Evaluation of Coalwash as a Potential Structural Fill Material for Port Reclamation. In Proceedings of the 12th Australia—New Zealand Conference on Geomechanics, Wellington, New Zealand, 22–25 February 2015.
38. Chiaro, G.; Indraratna, B.; Tasalloti, S.M.A. Predicting the behaviour of coal wash and steel slag mixtures under triaxial conditions. *Can. Geotech. J.* **2015**, *52*, 367–373. [CrossRef]
39. Rujikiatkamjorn, C.; Indraratna, B.; Chiaro, G. Compaction of coal wash to optimise its utilisation as water-front reclamation fill. *Geomech. Geoengin. Int. J.* **2013**, *8*, 36–45. [CrossRef]
40. Heitor, A.; Indraratna, B.; Kaliboullah, C.I.; Rujikiatkamjorn, C.; McIntosh, G.W. Drained and Undrained Shear Behavior of Compacted Coal Wash. *J. Geotech. Geoenviron. Eng.* **2016**, *142*, 04016006. [CrossRef]
41. Qi, Y.; Indraratna, B.; Vinod, J.S. Behavior of Steel Furnace Slag, Coal Wash, and Rubber Crumb Mixtures with Special Relevance to Stress–Dilatancy Relation. *J. Mater. Civ. Eng.* **2018**, *30*, 04018276. [CrossRef]
42. Indraratna, B.; Qi, Y.; Heitor, A. Evaluating the Properties of Mixtures of Steel Furnace Slag, Coal Wash, and Rubber Crumbs Used as Subballast. *J. Mater. Civ. Eng.* **2018**, *30*, 04017251. [CrossRef]
43. Tawk, M.; Qi, Y.; Indraratna, B.; Rujikiatkamjorn, C.; Heitor, A. Behavior of a Mixture of Coal Wash and Rubber Crumbs under Cyclic Loading. *J. Mater. Civ. Eng.* **2021**, *33*, 04021054. [CrossRef]
44. Tasalloti, S.M.A.; Indraratna, B.; Rujikiatkamjorn, C.; Heitor, A.; Chiaro, G. A Laboratory Study on the Shear Behavior of Mixtures of Coal Wash and Steel Furnace Slag as Potential Structural Fill. *Geotech. Test. J.* **2015**, *38*, 361–372. [CrossRef]
45. Chiaro, G.; Indraratna, B.; Tasalloti, S.M.A.; Rujikiatkamjorn, C. Optimisation of coal wash–slag blend as a structural fill. *Proc. Inst. Civ. Engineers. Ground Improv.* **2015**, *168*, 33–44. [CrossRef]
46. Xue, Y.; Wu, S.; Hou, H.; Zha, J. Experimental investigation of basic oxygen furnace slag used as aggregate in asphalt mixture. *J. Hazard. Mater.* **2006**, *138*, 261–268. [CrossRef]
47. Chien, H.-T.; Chang, J.-R.; Hsu, H.-M. Determining the content of steel furnace slag in asphalt concrete. *Case Stud. Constr. Mater.* **2023**, *19*, e02399. [CrossRef]
48. Pasetto, M.; Baliello, A.; Giacomello, G.; Pasquini, E. The Use of Steel Slags in Asphalt Pavements: A State-of-the-Art Review. *Sustainability* **2023**, *15*, 8817. [CrossRef]

49. Wang, D.; Tawk, M.; Indraratna, B.; Heitor, A.; Rujikiatkamjorn, C. A mixture of coal wash and fly ash as a pavement substructure material. *Transp. Geotech.* **2019**, *21*, 100265. [CrossRef]
50. Kim, B.; Prezzi, M.; Salgado, R. Geotechnical Properties of Fly and Bottom Ash Mixtures for Use in Highway Embankments. *J. Geotech. Geoenviron. Eng.* **2005**, *131*, 914–924. [CrossRef]
51. Baykal, G.; Edinçliler, A.; Saygılı, A. Highway embankment construction using fly ash in cold regions. *Resour. Conserv. Recycl.* **2004**, *42*, 209–222. [CrossRef]
52. Arulrajah, A.; Disfani, M.M.; Horpibulsuk, S.; Suksiripattanapong, C.; Prongmanee, N. Physical properties and shear strength responses of recycled construction and demolition materials in unbound pavement base/subbase applications. *Constr. Build. Mater.* **2014**, *58*, 245–257. [CrossRef]
53. Arulrajah, A.; Piratheepan, J.; Aatheesan, T.; Bo, M.W. Geotechnical Properties of Recycled Crushed Brick in Pavement Applications. *J. Mater. Civ. Eng.* **2011**, *23*, 1444–1452. [CrossRef]
54. Ahmad, F.; Mujah, D.; Hazarika, H.; Safari, A. Assessing the potential reuse of recycled glass fibre in problematic soil applications. *J. Clean. Prod.* **2012**, *35*, 102–107. [CrossRef]
55. Alfayez, S.A.; Suleiman, A.R.; Nehdi, M.L. Recycling Tire Rubber in Asphalt Pavements: State of the Art. *Sustainability* **2020**, *12*, 9076. [CrossRef]
56. Shu, X.; Huang, B. Recycling of waste tire rubber in asphalt and portland cement concrete: An overview. *Constr. Build. Mater.* **2014**, *67*, 217–224. [CrossRef]
57. Qi, Y.; Indraratna, B. Energy-Based Approach to Assess the Performance of a Granular Matrix Consisting of Recycled Rubber, Steel-Furnace Slag, and Coal Wash. *J. Mater. Civ. Eng.* **2020**, *32*, 04020169. [CrossRef]
58. Tawk, M.; Indraratna, B. Role of Rubber Crumbs on the Stress-Strain Response of a Coal Wash Matrix. *J. Mater. Civ. Eng.* **2021**, *33*, 04020480. [CrossRef]
59. Indraratna, B.; Qi, Y.; Tawk, M.; Heitor, A.; Rujikiatkamjorn, C.; Navaratnarajah, S.K. Advances in ground improvement using waste materials for transportation infrastructure. *Proc. Inst. Civ. Eng. Ground Improv.* **2022**, *175*, 3–22. [CrossRef]
60. Sol-Sánchez, M.; Thom, N.H.; Moreno-Navarro, F.; Rubio-Gámez, M.C.; Airey, G.D. A study into the use of crumb rubber in railway ballast. *Constr. Build. Mater.* **2015**, *75*, 19–24. [CrossRef]
61. Qiang, W.; Jing, G.; Connolly, D.P.; Aela, P. The use of recycled rubber in ballasted railway tracks: A review. *J. Clean. Prod.* **2023**, *420*, 138339. [CrossRef]
62. Qi, Y.; Indraratna, B. The effect of adding rubber crumbs on the cyclic permanent deformation of waste mixtures containing coal wash and steel furnace slag. *Géotech.* **2022**, *73*, 951–960. [CrossRef]
63. Indraratna, B.; Sun, Q.; Grant, J. Behaviour of subballast reinforced with used tyre and potential application in rail tracks. *Transp. Geotech.* **2017**, *12*, 26–36. [CrossRef]
64. Indraratna, B.; Sun, Q.; Heitor, A.; Grant, J. Performance of Rubber Tire-Confined Capping Layer under Cyclic Loading for Railroad Conditions. *J. Mater. Civ. Eng.* **2018**, *30*, 06017021. [CrossRef]
65. Indraratna, B.; Mehmood, F.; Ngo, T.; Rujikiatkamjorn, C.; Grant, J. Performance of Tire Cell Foundation as a Subballast Capping Layer under Cyclic Train Loading. *J. Geotech. Geoenviron. Eng.* **2025**, *151*, 04024134. [CrossRef]
66. Indraratna, B.; Ngo, T.; Bessa Ferreira, F.; Rujikiatkamjorn, C.; Shahkolahi, A. Laboratory examination of ballast deformation and degradation under impact loads with synthetic inclusions. *Transp. Geotech.* **2020**, *25*, 100406. [CrossRef]
67. Siddiqui, A.R.; Indraratna, B.; Ngo, T.; Rujikiatkamjorn, C. Laboratory assessment of rubber grid-reinforced ballast under impact testing. *Géotech. Lett.* **2023**, *13*, 118–128. [CrossRef]
68. Ngo, T.; Indraratna, B. Use of Geogrid for Improved Performance of Ballasted Tracks: Experimental and DEM Approaches. *Int. J. Geosynth. Ground Eng.* **2024**, *10*, 33. [CrossRef]
69. Mayuranga, H.G.S.; Navaratnarajah, S.K.; Bandara, C.S.; Jayasinghe, J.A.S.C. Elastic inclusions in ballasted tracks—A review and recommendations. *Int. J. Rail Transp. (Online)* **2024**, *12*, 253–280. [CrossRef]
70. Sol-Sánchez, M.; Moreno-Navarro, F.; Gámez, M. The use of deconstructed tire rail pads in railroad tracks: Impact of pad thickness. *Mater. Des.* **2014**, *58*, 198–203. [CrossRef]
71. Navaratnarajah, S.K.; Indraratna, B.; Ngo, N.T. Influence of Under Sleeper Pads on Ballast Behavior Under Cyclic Loading: Experimental and Numerical Studies. *J. Geotech. Geoenviron. Eng.* **2018**, *144*, 45–72. [CrossRef]
72. Navaratnarajah, S.K.; Indraratna, B. Use of Rubber Mats to Improve the Deformation and Degradation Behavior of Rail Ballast under Cyclic Loading. *J. Geotech. Geoenviron. Eng.* **2017**, *143*, 04017015. [CrossRef]
73. Alves Costa, P.; Calçada, R.; Silva Cardoso, A. Ballast mats for the reduction of railway traffic vibrations. Numerical study. *Soil Dyn. Earthq. Eng.* **2012**, *42*, 137–150. [CrossRef]
74. Jayasuriya, C.; Indraratna, B.; Ngoc Ngo, T. Experimental study to examine the role of under sleeper pads for improved performance of ballast under cyclic loading. *Transp. Geotech.* **2019**, *19*, 61–73. [CrossRef]
75. Indraratna, B.; Qi, Y.; Jayasuriya, C.; Rujikiatkamjorn, C.; Arachchige, C.M.K. Use of recycled rubber inclusions with granular waste for enhanced track performance. *Transp. Eng.* **2021**, *6*, 100093. [CrossRef]

76. Esmaeili, M.; Farsi, S.; Shamohammadi, A. Effect of rock strength on the degradation of ballast equipped with under sleeper pad. *Constr. Build. Mater.* **2022**, *321*, 126413. [CrossRef]
77. Riyad, A.S.M.; Indraratna, B.; Qi, Y.; Tawk, M. Constitutive behaviour of a granular matrix containing coal mine waste intermixed with rubber crumbs. *Acta Geotech.* **2024**, *20*, 185–196. [CrossRef]
78. Ahmed, I.; Lovell, C.W. *Rubber Soils as Lightweight Geomaterials*; Transportation Research Record No. 1422; Transportation Research Board: Washington, DC, USA, 1993; pp. 61–70.
79. Foose, G.J.; Benson, C.H.; Bosscher, P.J. Sand Reinforced with Shredded Waste Tires. *J. Geotech. Eng.* **1996**, *122*, 760–767. [CrossRef]
80. Edil, T.B.; Bosscher, P.J. Engineering Properties of Tire Chips and Soil Mixtures. *Geotech. Test. J.* **1994**, *17*, 453–464. [CrossRef]
81. Tatlisoz, N.; Edil, T.B.; Benson, C.H. Interaction between Reinforcing Geosynthetics and Soil-Tire Chip Mixtures. *J. Geotech. Geoenviron. Eng.* **1998**, *124*, 1109–1119. [CrossRef]
82. Ghazavi, M.; Sakhi, M.A. Influence of Optimized Tire Shreds on Shear Strength Parameters of Sand. *Int. J. Geomech.* **2005**, *5*, 58–65. [CrossRef]
83. Lee, J.; Salgado, R.; Bernal, A.; Lovell, C.W. Shredded Tires and Rubber-Sand as Lightweight Backfill. *J. Geotech. Geoenviron. Eng.* **1999**, *125*, 132–141. [CrossRef]
84. Zornberg, J.G.; Cabral, A.R.; Viratjandr, C. Behaviour of shred-sand mixtures. *Can. Geotech. J.* **2004**, *41*, 227–241. [CrossRef]
85. Mashiri, M.; Vinod, J.; Sheikh, M.N.; Tsang, H. Shear strength and dilatancy behaviour of sand–tyre chip mixtures. *Soils Found.* **2015**, *55*, 517–528. [CrossRef]
86. Sheikh, M.N.; Mashiri, M.S.; Vinod, J.S.; Tsang, H. Shear and Compressibility Behavior of Sand–Tire Crumb Mixtures. *J. Mater. Civ. Eng.* **2013**, *25*, 1366–1374. [CrossRef]
87. Ahmed, S.; Vinod, J.S.; Sheikh, M.N. Behavior of Sand–Tire Chip Mixtures in Constant Shear Drained Stress Path. *J. Mater. Civ. Eng.* **2022**, *34*, 04022294. [CrossRef]
88. Qi, Y.; Indraratna, B.; Heitor, A.; Vinod, J.S. Effect of Rubber Crumbs on the Cyclic Behavior of Steel Furnace Slag and Coal Wash Mixtures. *J. Geotech. Geoenviron. Eng.* **2018**, *144*, 04017107. [CrossRef]
89. Qi, Y.; Indraratna, B.; Vinod, J.S. Dynamic Properties of Mixtures of Waste Materials. In Proceedings of the GeoShanghai 2018 International Conference: Advances in Soil Dynamics and Foundation Engineering, Singapore, 27–30 May 2018; pp. 308–317.
90. Agustian, Y.; Goto, S. Strength and Deformation Characteristics of Scoria in Triaxial Compression at Low Confining Stress. *Soils Found.* **2008**, *48*, 27–39. [CrossRef]
91. Arachchige, C.M.K.; Indraratna, B.; Qi, Y.; Vinod, J.S.; Rujikiatkamjorn, C. Geotechnical characteristics of a Rubber Intermixed Ballast System. *Acta Geotech.* **2022**, *17*, 1847–1858. [CrossRef]
92. Qi, Y.; Indraratna, B.; Tawk, M. Use of Recycled Rubber Elements in Track Stabilisation. In Proceedings of the Geo Congress, Reston, VA, USA, 25–28 February 2020; pp. 49–59. [CrossRef]
93. Ahmed, I. *Laboratory Study on Properties of Rubber-Soils*; Indiana Department of Transportation, Purdue University: West lafayette, Indiana, 1993.
94. Youwai, S.; Bergado, D.T. Strength and deformation characteristics of shredded rubber tire. *Can. Geotech. J.* **2003**, *40*, 254–264. [CrossRef]
95. Anbazhagan, P.; Manohar, D.R.; Rohit, D. Influence of size of granulated rubber and tyre chips on the shear strength characteristics of sand-rubber mix. *Geomech. Geoengin. Int. J.* **2017**, *12*, 266–278. [CrossRef]
96. Masad, E.; Taha, R.; Ho, C.; Papagiannakis, T. Engineering Properties of Tire/Soil Mixtures as a Lightweight Fill Material. *Geotech. Test. J.* **1996**, *19*, 297–304. [CrossRef]
97. Lee, C.; Truong, Q.; Lee, W.; Lee, J. Characteristics of Rubber-Sand Particle Mixtures according to Size Ratio. *J. Mater. Civ. Eng.* **2010**, *22*, 323–331. [CrossRef]
98. Rao, G.V.; Dutta, R.K. Compressibility and Strength Behaviour of Sand–tyre Chip Mixtures. *Geotech. Geol. Eng.* **2006**, *24*, 711–724. [CrossRef]
99. Mashiri, M.; Vinod, J.; Sheikh, M.N. Constitutive Model for Sand–Tire Chip Mixture. *Int. J. Geomech.* **2016**, *16*, 04015022. [CrossRef]
100. Foriero, A.; Ghafari, N. Critical State Model of Sand-Tire Derived Aggregate Mixtures Based on Triaxial Tests. *Transp. Res. Rec.* **2021**, *2675*, 208–221. [CrossRef]
101. Cui, Z.-D.; Xu, M.-Z.; Wang, X.-D. Investigation of elastoplastic constitutive model of rubber-sand mixture. *Comput. Geotech.* **2025**, *177*, 106904. [CrossRef]
102. Qi, Y.; Indraratna, B.; Coop, M.R. Predicted Behavior of Saturated Granular Waste Blended with Rubber Crumbs. *Int. J. Geomech.* **2019**, *19*, 04019079. [CrossRef]
103. Duncan, J.; Byrne, P.; Wong, K.; Mabry, P. *Strength, Stress-Strain and Bulk Modulus Parameters for Finite Element Analyses of Stresses and Movements in Soil Masses*; College of Engineering, Office of Research Services, University of California: Berkeley, CA, USA, 1980.
104. El Naggar, H.; Ashari, M.; Mahgoub, A. Development of an empirical hyperbolic material model for TDA utilizing large-scale triaxial testing. *Int. J. Geotech. Eng.* **2022**, *16*, 133–142. [CrossRef]

105. Li, X.S.; Dafalias, Y.F. Dilatancy for cohesionless soils. *Géotechnique* **2000**, *50*, 449–460. [CrossRef]
106. Dafalias, Y.F. Bounding Surface Plasticity. I: Mathematical Foundation and Hypoplasticity. *J. Eng. Mech.* **1986**, *112*, 966–987. [CrossRef]
107. Been, K.; Jefferies, M.G. A state parameter for sands. *Géotechnique* **1985**, *35*, 99–112. [CrossRef]
108. Budhu, M. *Soil Mechanics and Foundations*, 3rd ed.; John Wiley & Sons: Chichester, UK, 2011.
109. Fu, R.; Coop, M.R.; Li, X.Q. The mechanics of a compressive sand mixed with tyre rubber. *Géotech. Lett.* **2014**, *4*, 238–243. [CrossRef]
110. Disfani, M.M.; Tsang, H.-H.; Arulrajah, A.; Yaghoubi, E. Shear and Compression Characteristics of Recycled Glass-Tire Mixtures. *J. Mater. Civ. Eng.* **2017**, *29*, 06017003. [CrossRef]
111. Li, J.; Cui, J.; Shan, Y.; Li, Y.; Ju, B. Dynamic Shear Modulus and Damping Ratio of Sand–Rubber Mixtures under Large Strain Range. *Materials* **2020**, *13*, 4017. [CrossRef] [PubMed]
112. Qi, Y.; Indraratna, B.; Heitor, A.; Vinod, J.S. Closure to “Effect of Rubber Crumbs on the Cyclic Behavior of Steel Furnace Slag and Coal Wash Mixtures” by Yujie Qi, Buddhima Indraratna, Ana Heitor, and Jayan S. Vinod. *J. Geotech. Geoenviron. Eng.* **2019**, *145*, 07018035. [CrossRef]
113. Qi, Y.; Indraratna, B.; Ngo, T.; Ferreira, F.B. Advancements in Geo-Inclusions for Ballasted Track: Constitutive Modelling and Numerical Analysis. *Sustainability* **2021**, *13*, 9048. [CrossRef]
114. Indraratna, B.; Rujikiatkamjorn, C.; Tawk, M.; Heitor, A. Compaction, degradation and deformation characteristics of an energy absorbing matrix. *Transp. Geotech.* **2019**, *19*, 74–83. [CrossRef]
115. Jefferies, M.; Been, K. *Soil Liquefaction: A Critical State Approach*, 2nd ed.; CRC Press: Milton, FL, USA, 2016.
116. Nova, R.; Wood, D. A constitutive model for soil under monotonic and cyclic loading. *Soil Mech. Transient Cycl. Load.* **1982**, *28*, 343–373.